

1 Wave Climate in a Shallow Estuary of a Rapidly Eroding Coast

2 Ranjit Jadhav<sup>1</sup>, Qin Chen<sup>1\*</sup>, and Weiming Wu<sup>2</sup>

3

4 <sup>1</sup>Department of Civil and Environmental Engineering, Louisiana State University, Baton Rouge,  
5 LA 70803, USA.

6 <sup>2</sup>National Center for Computational Hydroscience and Engineering, The University of  
7 Mississippi, University, MS 38677, USA.

8 \*Corresponding Author

9

10 Emails and Phones: rjadha1@lsu.edu, +1-225-578-6588

11 qchen@lsu.edu, +1-225-578-4911

12 wuwm@ncche.olemiss.edu, +1-662-915-6561

13

14 Abstract

15 Coastal ecosystems such as the deltaic salt-marshes and the adjacent shallow estuaries of  
16 Louisiana on the northern Gulf of Mexico are some of the most productive and threatened  
17 ecosystems of the world. Wave energy has been noted as an important factor in salt marsh  
18 erosion but unlike ocean environments, long term wave monitoring data typically do not exist for  
19 estuarine systems. Using seven months of directional wave measurements spanning all seasons,  
20 this study examines the extent of wave energy present in rapidly eroding Terrebonne Bay. Wind  
21 seas are the dominant wave energy in the bay producing bed shear stresses that exceed critical  
22 sediment re-suspension value 20-30% of the time. In the northern marshes of the study area, the  
23 estimated retreat rates based on wave power calculations are up to 10 m/yr in agreement with the

24 recent monitoring data. Swell frequently enter bay through the gaps in the natural barrier islands.  
25 The ratio of the swell induced bed shear stress to the sea induced shear stress is found to be 2 to  
26 4 times higher than corresponding ratio of swell energy to sea energy. Measured offshore swell  
27 reduce to 25% in wave height inside bay at the measurement site. Considering the  
28 disproportionately larger bed shear stresses produced by low energy swell, it is critical to restore  
29 and maintain the coastal barrier islands to limit erosion in the bays. The presented wind sea and  
30 swell data will help in engineering restoration and protection strategies for the vanishing  
31 wetlands.

## 32 **1 Introduction**

33

34 Coastal ecosystems are some of the most productive and threatened ecosystems in the  
35 world [Lotze *et al.* 2006; Halpern *et al.* 2008]. They comprise of salt marshes, coral reefs,  
36 mangroves, and seagrasses and provide important ecological and economic values [e.g.  
37 Costanza, 1997]. An estimated 50% of salt marshes, 35% of mangroves, 30% of coral reefs, and  
38 29% of seagrasses are either lost or degraded worldwide [Barbier *et al.*, 2011 and references  
39 therein]. The loss has resulted in 33% decline in the number of viable fisheries; 69% decline in  
40 the provision of nursery habitats such as oyster reefs, seagrass beds, and wetlands; and 63%  
41 decline in filtering and detoxification services provided by suspension feeders, submerged  
42 vegetation, and wetlands [Worm *et al.*, 2006].

43 In the world's major deltaic plains the loss has been estimated to be 95 km<sup>2</sup>/yr over the  
44 past 14 years [Coleman *et al.*, 2008]. Mississippi River delta in Louisiana has particularly  
45 experienced dramatic wetland loss. Between 1956 and 2006, annual land loss rates ranged from  
46 34 km<sup>2</sup>/yr to 104 km<sup>2</sup>/yr. Average annual land loss rate over that time period was approximately

47 70 km<sup>2</sup>/yr [Barras *et al.*, 2003]. This loss represents 80% of the coastal wetland loss in the entire  
48 continental United States. The public use value of this loss is estimated to be in excess of \$37  
49 billion by 2050 [LCWCRTF, 1998].

50 On the Louisiana coast, the reasons for wetland loss are complex and both natural and  
51 anthropogenic [Day *et al.*, 2000; Gagliano, 2003; Morton *et al.*, 2006]. One of the important  
52 causes of erosion is the constant wave action along the marsh edges. Analysis by Penland *et al.*  
53 (2000) showed that 26% of the wetland loss in the Mississippi river delta from 1932 to 1990 can  
54 be attributed to erosion due to wind waves.

55 Wind waves also influence sediment re-suspension in the nearshore area [Sanford, 1994;  
56 Sheremet *et al.*, 2005; Kineke *et al.*, 2006; Jaramillo *et al.*, 2009]. Wind waves have been shown  
57 to play important role in the morphological evolution of intertidal regions [Defina *et al.*, 2007;  
58 Fagherazzi *et al.*, 2007; Fagherazzi and Wiberg, 2009]. Kirby (2000) noted that the shape of the  
59 mudshore profile is controlled by tidal currents and particularly by wave climate. Importantly,  
60 wind waves degrade salt marsh through scarp erosion [Tonelli *et al.*, 2010]. The role of wave  
61 attack on coastal marshes is compounded by the conversion of marsh platforms to open-water,  
62 thereby increasing the fetch and wave forces on exposed marsh edges.

63 On the Louisiana-Mississippi coast, the marshes are typically protected by barrier islands.  
64 When the barrier islands disappear, so do the marshes mainly because of the wave-induced  
65 damage and erosion. Studies have found a strong correlation between the level of wave energy  
66 and the survival of wetland marshes [e.g. Roland and Douglass, 2005].

67 The Northern coast of Gulf of Mexico annually experiences tropical storms and  
68 hurricanes and the coastal wetlands provide a natural first line of defense against approaching

69 storm surge and waves [e.g. *Lopez*, 2009]. By one estimate, in the US, the coastal wetlands were  
70 estimated to provide \$23.2 billion in storm protection services annually [*Costanza*, 2008].

71 In this study we investigate the characteristics of the wave environment in Terrebonne  
72 Bay, a rapidly eroding shallow estuary on the fragile Gulf coast of Louisiana. Analyzing  
73 directional wave gage data collected over a period of 7 months, we examine the extent of wave  
74 energy and bed shear stresses affecting the bay and the fringing eroding salt marshes. Isolating  
75 the low frequency swell energy from bimodal spectra, we examine the level of resulting bed  
76 shear stresses in comparison with the more conspicuous wind wave induced bed shear stresses.  
77 Most Louisiana estuaries are partially sheltered from offshore wave energy by bordering barrier  
78 islands. This sheltering effect is one of the main reasons for a barrier island restoration program  
79 in the region [CPRA, 2007]. The important benefit of barrier islands in mitigating wave field in  
80 the back bays has been demonstrated using numerical models [e.g. *Stone et al.*, 2005]. However,  
81 to the authors' knowledge no long term field measurements exist to quantify this benefit. With  
82 field measurements, we quantify the reduction in swell height by comparing offshore and  
83 bayside measurements. Based on wave power calculations, we estimate marsh retreat rates in  
84 comparison with the recent monitoring data in the area

## 85 **2 Study Area**

86  
87 Terrebonne Bay is a shallow estuary on the Louisiana coast of Northern Gulf of Mexico  
88 on the west side of the mouth of the Mississippi River (Figure 1). Although part of the  
89 abandoned deltaic lobes, currently the basin receives no major fluvial discharge. The bay is  
90 bounded by the natural levees of Bayou Terrebonne on the east and the Houma Navigation Canal  
91 on the west. Salt marshes line the upper portions of the bay with vegetation communities of

92 smooth cordgrass (*Spartina alterniflora*) and saltmarsh meadow (*Spartina patens*). On the south,  
93 the bay is bordered a series of narrow, low-lying barrier islands of the Isles Dernieres and the  
94 Timbalier Islands. The wave environment in the bay comprised of generally locally generated  
95 seas but offshore swell do propagate inwards through the gaps in the barrier island chain. The  
96 region has a microtidal environment (tide < 0.5 m) and depths in the bay vary from 1 to 3 m.  
97 Fetch mainly exists in the southeast quadrant and varies between 10 to 24 km. Every year from  
98 October to April about 30 to 40 cold weather fronts pass through the region [Moeller *et al.*,  
99 1993]. A typical front lasts from 3-7 days when winds build up from the southerly quadrants and  
100 then turn clockwise to strong northerly winds. The dominant wind directions are southeast and  
101 northwest. The region also experiences tropical storms and hurricanes annually, but none  
102 occurred during the data collection period of the present study.

### 103 **3 Instrumentation, Data and Analysis**

104

105 Directional data in the bay was collected using an acoustic doppler velocimeter, Sontek  
106 Triton-ADV Wave/ Tide/ Current Gauge (ADV). The ADV was deployed at 29°11'13.20"N  
107 90°36'33.59"W, approximately 10 km north of the Timbalier Islands (ADV in Figure 1). To the  
108 south of this location, outside the barrier island chain, at approximately 15 km, wave gage CSI-  
109 05 collects hourly non-directional wave parameters. The ADV location has a limited fetch from  
110 northwest to southwest. However, it is directly to the north of Cat Island Pass which provides a  
111 break in the barrier island chain allowing low energy swell to propagate northwards in the bay.  
112 Over the periods from February 23, 2010 through April 29, 2010 and from July 24, 2010 through  
113 February 14, 2011, 17 min bursts were sampled at 4 Hz frequency every 30 minutes to record  
114 puv (pressure, x-component of velocity and y-component of velocity) time series. The wave

115 records were analyzed using standard spectral methods to produce integral parameters of (zero  
116 moment) wave height,  $H_{mo}$ , and peak period,  $T_p$ . For the analysis presented in this paper, sea and  
117 swell records exceeding 0.05 m in wave height were only considered. This subset represents  
118 about 40% of the 7 month dataset.

119 A large percentage of wave spectra measured in the bay, showed presence of low  
120 frequency swell (Figure 2 bottom panel, reddish brown low frequency bands). To examine the  
121 wind wave and swell characteristics, all the bimodal spectra were further partitioned into sea and  
122 swell. Starting with the conceptual algorithm of *Gerling* (1992) several partitioning schemes  
123 [e.g. *Voorrips et al.*, 1997, *Hanson and Phillips*, 2001] have been developed. Various schemes in  
124 the literature differ primarily in the strategies to combine peaks in a multimodal spectrum and  
125 use arbitrary criteria [*Portilla et al.*, 2009]. In the present study, majority of the measured  
126 bimodal wave spectra exhibited relatively distinct low and high frequency energy peaks. To  
127 partition the spectra following procedure was adopted. First, spurious peaks in the high  
128 frequency region were replaced by applying a tail with exponent -4 starting from  $1.2*fp$  (peak  
129 frequency). Second, spurious peaks in the low frequency region were ignored by truncating  
130 spectrum below frequency 0.05 Hz. Third, the highest two peaks in the spectrum were identified  
131 provided that they were separated by at least a frequency difference of  $1.2*fp$  from each other.  
132 Finally, the spectrum was split at the lowest point between the two peaks, provided the lowest  
133 point was 85% of the smaller peak.

#### 134 **4 Wind Wave and Swell Climate** 135

136 An example of wind and wave field produced by a typical winter front during our study is  
137 shown in Figure 2. Spectral wave heights ( $H_{mo}$ ) of smaller than 0.1 m are not plotted, however,

138 corresponding peak periods ( $T_p$ ) are shown to identify and emphasize the presence of swell. At  
139 the beginning of the front, when winds are calm (25-Oct), low energy swell enter the bay and sea  
140 is negligible. As winds start building up from the south (on 26-Oct), wind waves slowly increase  
141 in wave heights to around 0.4 m and peak periods between 2.7-2.9 sec. In the subsequent days,  
142 although the winds continue to blow from south, the speeds are low (around 5 m/s), resulting in  
143 no significant wind waves. The swell however continues to be present throughout. As the winds  
144 turn clockwise and start blowing from (28-Oct), swell energy subsides. As there is no fetch to the  
145 north of the ADV station, no significant waves are produced. The intensity and nature (long or  
146 short) of the wave field in the bay can be seen in the statistical distributions of the entire wave  
147 height and period data set (Figure 3a). In case of swell, the average spectral wave height was  
148 0.10 m while average peak period was 6.9 sec. Over the entire data set, sea spectral height  
149 average was 0.29 m and the average peak period was 2.7 sec. Wind wave field was primarily  
150 generated from the southeast quadrant with northeast being the secondary dominant direction.  
151 The swell largely approached from the directions between  $150^\circ$  to  $170^\circ$  (meteorological  
152 convention).

153 To investigate the influence of swell compared to that of wind waves in inducing  
154 sediment re-suspension, bed shear stresses resulting from these two forcings were examined  
155 separately. Assuming linear wave theory is valid, the maximum bottom orbital velocity,  $u_b$ , can  
156 be calculated by

$$u_b = \frac{\pi H}{T \sinh(kh)} \quad (1)$$

157 where  $H$  is wave height,  $T$  is wave period,  $k$  is wave number and  $h$  is the depth.

158 The bed shear stress,  $\tau$ , can be then computed as,

$$\tau = \frac{1}{2} f_w \rho u_b^2 \quad (2)$$

159 where,  $f_w$ , is the friction factor expressed as,

$$f_w = 0.04 \left( \frac{u_b T}{2\pi k_s} \right)^{-0.25} \quad (3)$$

160 Friction factor,  $f_w$ , depends on the grain roughness scale,  $K_s$ , which can be calculated  
 161 using  $K_s = 2.5 * D_{50}$  [Fredsoe and Deigaard, 1993]. The predominant sediment types in the bay  
 162 are sandy silt and clayey silt with  $D_{50} = 0.025$  mm [Perret et al., 1971].

163 Figure 4a shows the relative contribution of swell and sea induced bed shear stress  
 164 compared to the corresponding relative energy over the entire data set. Size of the symbols  
 165 indicate, spectral wave height ( $H_{mo}$ ) estimated from the un-partitioned spectra. Generally, during  
 166 the low energy wave field in “shallower” regimes (small, blue dots), both the shear stress and  
 167 wave energy ratios are comparable (closer to 1:1 line). As the regime becomes less shallower  
 168 while wave energy still low (small, cyan dots), shear stress ratio becomes 1.5 to 2 times of the  
 169 energy ratio. For low energy, less shallow regimes (small, brown dots), the shear stress ratio is  
 170 more than 4 times that of the wave energy ratio, indicating disproportionately higher role of  
 171 swell in inducing bed shear stress compared to the corresponding energy level ratios. Also note  
 172 that, low energy (small dots) events largely fall in to the region when  $E_{swell}/E_{sea} > 1$  indicating  
 173 swell presence in low winds. Most high energy events (large dots) fall in the region where  
 174  $E_{swell}/E_{sea} < 0.5$  where seas are dominating in terms of energy. However, in terms of bed shear  
 175 stress, swell appear to contribute 1.5 (“shallower” regime) to 4 (“less shallower” regime) times  
 176 more than the seas. As an example, when swell energy component is only 20% of the sea energy,  
 177 the resulting swell shear stress is 30 to 90% of the sea shear stress depending on the “depth”  
 178 experienced by the wave field.

179 To examine the exceedance probability of bed shear stresses, cumulative statistics is  
180 presented in Figure 4b. The total stress is computed by vector summation of sea and swell  
181 stresses using dominant wave direction for each component obtained from the directional spectra  
182 [Camenen and Larson, 2005]. Measurements of critical bed shear stress,  $\tau_{cr}$ , were not available  
183 in the study area, however, the shaded region shows generally accepted range from the literature  
184 [Lund-Hansen et al., 2004; Wang, 2003; Wright et al., 1997; Xu et al., 2011]. It can be seen that  
185 the critical bed shear stress exceeded for 50-80% of the data (20-30% of the study duration  
186 because analyzed data represents 40% of the collected values). In terms of absolute magnitude,  
187 in the current physical setting (extent of barrier island gaps, bay bathymetry), swell induced  
188 shear stresses are much less than the sea induced shear stresses. The total stress exceedance  
189 curve does not differ significantly from the dominant sea stress curve due to two reasons. First,  
190 the contribution from swell stress is smaller in magnitude. Second, as shown in Figure 3c, the  
191 dominant sea stress direction ( $120^{\circ}$ - $130^{\circ}$ ) is different from the dominant swell stress direction  
192 ( $160^{\circ}$ - $170^{\circ}$ ) which precludes linear addition of two components in most events. However, it  
193 should be noted that, about 10% swell entered from directions between  $130^{\circ}$ - $140^{\circ}$  where a gap in  
194 the barrier island system exists. If this gap widens and remains un-restored, intruding swell will  
195 enhance shear stresses produced by winds waves in this meteorologically dominant direction.  
196 Bed shear stress is directly related to the erosion potential in the bay. The relative contribution of  
197 swell induced shear stress based on the long term observed data presented here underlines the  
198 importance of this silent forcing. With the unabated loss of barrier island systems, the swell  
199 penetration is only expected to increase exacerbating erosion potential of the system.

200 To investigate, the protection provided by the barrier islands, we compared swell height  
201 measured offshore to that measured at our site, ADV, in the bay. Figure 5 shows the fraction of

202 swell height propagated into the bay for a given incident swell over the entire data collection  
203 periods. To represent offshore incident swell, spectral significant wave heights ( $H_o$ ) for which  
204 the peak time period was larger than 5 sec ( $f_p < 0.2$  Hz) were selected from the observations  
205 reported at station CSI-05. Figure 5 shows that swell heights reduce to at least 25% up to the  
206 ADV station. This reduction is the result of processes of diffraction, refraction and dissipation  
207 through bottom friction. Barrier islands play an important role of sheltering the inner bay. Note  
208 that the data presented is from a fixed location; actual swell energy will have spatial variation.

209 In addition to bay erosion, we examined potential for the landward retreat of the marsh  
210 edge caused by attacking waves. Wave power,  $P_w = E \cdot C_g$ , where  $E$  is the wave energy and  $C_g$  is  
211 the group velocity, was computed for each measurement. Wave power in a given direction was  
212 then summed over the entire data set. It was related to marsh edge retreat rate following  
213 *Schwimmer* (2001) as shown in Figure 6. Although, the wave power estimates are based on  
214 measurements about 4 km away from the marsh edge and the possibility of differing retreat rate  
215 relation than that proposed by *Schwimmer* (2001), the estimates indicate grave retreat potential.  
216 At three sites in the northern marsh edges of the bay, during the period from 1998- to 2005, the  
217 retreat rate averaged 3-6 m/yr (CPRA, 2010) which agrees well with our estimates. In addition to  
218 the relentless wind wave action, the marsh edge is also subject to persistent swell as captured by  
219 our data. Studies have shown that the long waves produce strong swash currents resulting in  
220 marsh substrate detachment [*Priestas and Fagherazzi*, 2011]. The phenomenon is in agreement  
221 with our observations of triangular wave-cut gullies at the area marsh sites.

## 222 5 Discussion and Conclusions

223

224 Directional wave measurements were carried out inside a rapidly eroding shallow bay  
225 partially protected by barrier islands to quantify the intensity and nature of the wave field. In  
226 addition to dominant seas, frequent swell energy was observed. For swell, the average spectral  
227 wave height was 0.10 m while average peak period was 6.9 sec. As observed from the regional  
228 meteorology, the dominant wind direction was 120°-130°. The dominant swell stress direction  
229 was 160°-170° where a gap in the barrier island is present. About 10% of the swell entered from  
230 130°-140° direction where another gap is located. Analysis showed that while low in energy,  
231 swell contribute disproportionately higher to the bed shear stress. The proportion of swell  
232 contribution increase markedly when wind sea experiences “deeper” regime. Importance of swell  
233 in estuaries, including the intertidal zone has also been illustrated by studies in San Francisco  
234 Bay [Talke and Stacey, 2003], Chesapeake Bay [Boon et al., 1996] and Cleveland Bay in  
235 Australia [Jing and Ridd, 1998]. The estimated bed shear stress exceeded critical shear stress for  
236 erosion in 20-30% of the measurements of the entire study period.

237 To the authors’ knowledge, these were the first long term measurements (over 7 months  
238 periods) inside an estuary of this fragile coast where erosion and land loss has reached  
239 catastrophic proportion and threatened commercial, recreational and community well being.  
240 Reliable quantification of wave environment, is an important piece in understanding physical  
241 processes and in developing erosion mitigation solutions which require significant financial  
242 resources. For example, knowledge of quantified wave environment is important in sediment  
243 deposition on the salt-marshes. The deposition depends on both the availability (created by  
244 waves) of suspended sediment and the opportunity (created by wind-induced high water levels)  
245 for that sediment to be transported over the marsh [Reed, 1989]. An example of importance of  
246 quantified wave environment for coastal protection projects is found in the in the northern

247 marshes of our study area. In this area, the Louisiana State Office of Coastal Protection and  
248 Restoration (OCPR) has invested over one and half million US dollars to evaluate shoreline  
249 protection treatment (e.g. gabion mats) and to enhance oyster habitat (CPRA, 2010). Our  
250 estimates of marsh retreat in this area based on wave power, show grave potential in the northern  
251 marshes and are consistent with the OCPR monitoring data. Reliable wave data would be critical  
252 to design of such systems in estuaries.

253         Bed shear stress is directly related to the erosion potential of the bay and fringing  
254 marshes. In addition to the wind wave induced bed shear stresses, the relative contribution of  
255 swell induced shear stresses is important. While the local wind sea environment cannot be  
256 controlled, swell penetration can be limited by restoring and maintaining the natural barrier  
257 islands.

258         The presented data can be used to test numerical models of waves in shallow estuaries;  
259 validated numerical models is an important tool to predict waves near wetlands. For the coastal  
260 engineers and coastal scientists involved in developing wetland protection measures, the results  
261 underscore the severity of marsh retreat potential and importance of considering oceanic swell in  
262 shallow bays. For coastal ecologists involved in the salt-marsh deterioration and sediment  
263 delivery; for estuarine geomorphologists studying intertidal mudflat evolution; for biologists  
264 concerned about shellfish colonization and habitats, our results provide the magnitudes of wave  
265 energy as an important driving force.

## 266 **Acknowledgements** 267

268         The study has been supported by the US Department of Homeland Security (DHS)  
269 through the Southeast Region Research Initiative (SERRI) and by the US National Science

270 Foundation (NSF) (Grant No. 0652859). We thank the Field Support Group of the Coastal  
271 Studies Institute of LSU for assisting in bayside wave data collection, WAVCIS group for  
272 providing offshore wave data and the LUMCON for providing the meteorological data. Any  
273 opinions, findings and conclusions or recommendations expressed in this paper are those of the  
274 authors and do not necessarily reflect the views of the NSF or the DHS.

275 **REFERENCES**

276

- 277 Barbier, E.B., S.D. Hacker, C. Kennedy, E.W. Koch, A.D. Stier, and B.R. Silliman (2011), The  
278 value of estuarine and coastal ecosystem services, *Ecological Monographs*, 81, 169–193.
- 279 Barras, J., S. Beville, D. Britsch, S. Hartley, S. Hawes, J. Johnston, P. Kemp, Q. Kinler, A.  
280 Martucci, J. Porthouse, D. Reed, K. Roy, S. Sapkota, and J. Suhayda (2003), Historical  
281 and projected coastal Louisiana land changes: 1978-2050: USGS Open File Report 03-  
282 334, 39 p. (Revised January 2004).
- 283 Boon, J.D., M.O. Green and K.D. Suh (1996) , Bimodal wave spectra in lower Chesapeake Bay,  
284 sea bed energetics and sediment transport during winter storms. *Cont. Shelf Res.*, 16,  
285 1965–1988.
- 286 Camenen, B., M. Larson (2005), A general formula for non-cohesive bed load sediment  
287 transport. *Estuarine, Coastal and Shelf Sci.*, 63, 249-260.
- 288 Coleman, J.M., O.K. Huh and D. Braud, Jr. (2008), Wetland loss in world deltas, *J. Coastal Res.*,  
289 24(1A), 1–14.
- 290 Costanza R, et al. (1997), The value of the world’s ecosystem services and natural capital,  
291 *Nature*, 387, 253–260.

292 Costanza, R., O. Pe´rez-Maqueo, M.L. Martinez, P. Sutton, S.J. Anderson and K. Mulder (2008),  
293 The value of coastal wetlands for hurricane protection, *Ambio*, 37, 241–248.

294 CPRA (Coastal Protection and Restoration Authority of Louisiana) (2007), Integrated ecosystem  
295 restoration and hurricane protection: Louisiana’s comprehensive master plan for a  
296 sustainable coast. Baton Rouge, Louisiana.

297 CPRA (2010), Operations, Maintenance, and Monitoring Report for Terrebonne Bay Shore  
298 Protection Demonstration (TE-45). Baton Rouge, Louisiana.

299 Day, J., L. Britsch, S. Hawes, G. Shaffer, D. Reed, and D. Cahoon (2000), Pattern and process of  
300 land loss in the Mississippi delta: a spatial and temporal analysis of wetland habitat  
301 change. *Estuaries* 23 (4), 425–438.

302 Defina, A., L. Carniello, S. Fagherazzi, and L. D’Alpaos (2007), Self organization of shallow  
303 basins in tidal flats and salt marshes, *J. Geophys. Res.*, 112, F03001.

304 Fagherazzi S., C. Palermo, M.C. Rulli, L. Carniello, and A. Defina (2007), Wind waves in  
305 shallow microtidal basins and the dynamic equilibrium of tidal flats, *J. Geophys. Res.*,  
306 112(F2); F02024.

307 Fagherazzi, S., and P. L. Wiberg (2009), Importance of wind conditions, fetch, and water levels  
308 on wave-generated shear stresses in shallow intertidal basins, *J. Geophys. Res.*, 114,  
309 F03022.

310 Fredsoe, J., and R. Deigaard (1993), Mechanics of Coastal Sediment Transport, *Adv. Ser. Ocean*  
311 *Eng.*, vol. 3, 392 pp., World Sci., Singapore.

312 Gagliano, S. (2003), Neo-tectonic framework of southeast Louisiana and applications to coastal  
313 restoration, *Transactions-Gulf Coast Association of Geological Societies*, 53, 262–276.

314 Gerling, T.W. (1992), Partitioning sequences and arrays of directional wave spectra into  
315 component wave systems, *J. Atm. Oceanic Tech.*, 9, 444-458.

316 Halpern, B. S., et al. (2008), A global map of human impacts on marine ecosystems, *Science*  
317 319, 948–952.

318 Hanson, J. L., and O. M. Phillips (2001), Automated analysis of ocean surface directional wave  
319 spectra, *J. Atm. and Oceanic Tec.*, 18, 277–293.

320 Jaramillo, S., A. Sheremet, M. A. Allison, A. H. Reed, and K. T. Holland (2009), Wave-mud  
321 interactions over the muddy Atchafalaya subaqueous cliniform, Louisiana, United States:  
322 Wave-supported sediment transport, *J. Geophys. Res.*, 114, C04002.

323 Jing, L., and P.V. Ridd (1996), Wave–current bottom shear stresses and sediment re-suspension  
324 in Cleveland Bay, Australia. *Coastal Eng.* 29, 169–186.

325 Kineke, G. C., E.E. Higgins, K. Hart, and D. Velasco (2006), Fine-sediment transport associated  
326 with cold front passages on the shallow shelf, Gulf of Mexico, *Cont. Shelf Res.*, 26,  
327 2073–2091.

328

329 Kirby, R. (2000), Practical implications of tidal flat shape, *Cont. Shelf Res.*, 20, 1061– 1077.

330

331 LCWCRTF (1998), Louisiana Coastal Wetlands Conservation and Restoration Task Force, 1998.  
332 Coast 2050: Toward a Sustainable Coastal Louisiana. Louisiana Department of Natural  
333 Resources, Baton Rouge, LA. Available online: <http://www.coast2050.gov/report.pdf>.

334 Lopez, J.A. (2009), The Multiple Lines of Defense Strategy to Sustain Coastal Louisiana, *J.*  
335 *Coastal Res.: Special Issue 54 - Geologic and Environmental Dynamics of the*  
336 *Pontchartrain Basin [FitzGerald & Reed]: pp. 186 – 197.*

337 Lotze, H. K., H.S. Lenihan, B.J. Bourque, R.H. Bradbury, R.G. Cooke, M.C. Kay, S.M. Kidwell,  
338 M.X. Kirby, C.H. Peterson, and J.B.C. Jackson (2006), Depletion, degradation, and  
339 recovery potential of estuaries and coastal seas, *Science*, 312, 1806–1809.

340 Lund-Hansen, L.C., M. Pejrup, and S. Fløderus (2004), Pelagic and seabed fluxes of  
341 particulate matter and carbon, and C:N ratios resolved by sediment traps during a spring  
342 bloom, southwest Kattegat, *J. of Sea Res.*, 52, 87–98.

343 Moeller, C.C., O. K. Huh, H.H. Roberts, L.E. Gumley and W.P. Menzel (1993), Response of  
344 Louisiana coastal environments to a cold front passage, *J. Coastal Res.*, 9 (2), 434–447.

345 Morton, R., J. Bernier, and J. Barras (2006), Evidence of regional subsidence and associated  
346 interior wetland loss induced by hydrocarbon production, Gulf coast region, USA,  
347 *Environmental Geology*, 50, 261–274.

348 OCPR (2010), Terrebonne Bay Shore Protection Demonstration (TE-45), Operations,  
349 Maintenance, and Monitoring Report, Office of Coastal Protection and Restoration,  
350 Louisiana Department of Natural Resources, Baton Rouge, Louisiana.

351 Penland, S., L. Wayne, L. Britsch, S. Williams, A. Beall, and V. Butterworth (2000), Process  
352 Classification of Coastal Land Loss between 1932 and 1990 in the Mississippi River  
353 Delta Plain, Southeastern Louisiana. U.S. Geological Survey Open File Report 00–418.

354 Perret, W. S., Barrett, B. B., Latapie, W. R., Pollard, J. F., Mock, W. R., Adkins, G. B., Gaidry,  
355 W. J. & White, C. J. (1971). Cooperative Gulf of Mexico Estuarine Inventory and Study,  
356 Louisiana. Phase I, Area Description and Phase IV, Biology. New Orleans, LA:  
357 Louisiana Wildlife and Fisheries Commission.

358 Portilla, J., F. O. Torres, and J. Monbaliu (2009), Spectral partitioning and identification of wind  
359 sea and swell, *J. Atm. and Oceanic Tech.*, 26, 107–122.

360 Priestas, A.M., and S. Fagherazzi (2011), Morphology and hydrodynamics of wave-cut gullies,  
361 *Geomorphology*, 131, 1–13.

362 Reed, D.J. (1989), Patterns of sediment deposition in subsiding coastal salt marshes, Terrebonne  
363 Bay, Louisiana: the role of winter storms. *Estuaries* 12:222–7.

364 Roland. R. M. and S.L. Douglass (2005), Wave tolerance of *spartina alterniflora* in coastal  
365 Alabama, *J. Coastal Res.*, 21, 453-463.

366 Sanford, L. P. (1994), Wave-forced resuspension of upper Chesapeake Bay muds, *Estuaries*  
367 17(18), 148–165.

368 Schwimmer, R. A. (2001), Rates and processes of marsh shoreline erosion in Rehoboth Bay,  
369 Delaware, U.S.A., *J. Coastal Res.*, 17(3), 672–683.

370 Sheremet, A., A. J. Mehta, B. Liu, and G. W. Stone (2005), Wave-sediment interaction on a  
371 muddy inner shelf during Hurricane Claudette, *Estuarine Coastal Shelf Sci.*, 63, 225–  
372 233.

373 Stone, G.W., Zhang, X., and Sheremet, A., 2005, The role of barrier islands, muddy shelf, and  
374 reefs in mitigating the wave field along Coastal Louisiana, in Finkl, C.W., and Khalil, S.,  
375 eds., Saving America’s wetland: Strategies for restoration of Louisiana’s coastal wetlands  
376 and barrier islands, *J. Coastal Res.*, *Special Issue 44*, p. 40–55.

377 Talke, S.A. and M.T. Stacey (2003), The influence of oceanic swell on flows over an estuarine  
378 intertidal mudflat in San Francisco Bay, *Est. Coastal, and Shelf Sci.* 58, 541-554.

379 Tonelli, M., S. Fagherazzi, and M. Petti (2010), Modeling wave impact on salt marsh boundaries.  
380 *J. Geophys. Res.* 115, C09028.

381 Voorrips, A. C., V. K. Makin, and S. Hasselmann (1997), Assimilation of wave spectra from  
382 pitch-and-roll buoys in a North Sea wave model, *J. Geophys. Res.*, 102, 5829–5849.

383 Wang, Y.H. (2003), The intertidal erosion rate of cohesive sediment: a case study from Long  
384 Island Sound Estuarine, *Coastal and Shelf Sci.*, 56, 891–896.

385 Worm, B., et al. (2006), Impacts of biodiversity loss on ocean ecosystem services, *Science*, 314,  
386 787–790.

387 Wright, L.D., C.R. Sherwood, and R.W. Sternberg (1997), Field measurements of fair-weather  
388 bottom boundary layer processes and sediment suspension on the Louisiana inner  
389 continental shelf. *Marine Geology*, 140, 329–345.

390 Xu, K., C.K. Harris, R.D. Hetland, and J.M. Kaihatu (2011), Dispersal of Mississippi and  
391 Atchafalaya sediment on the Texas–Louisiana shelf: Model estimates for the year 1993.  
392 *Cont. Shelf Res.*, in press.

393

394 Figure Captions

395

396 Figure 1 Study area, bathymetry and locations of monitoring gages

397

398 Figure 2 Measured wave heights and periods at ADV (bay) and CSI-05 (offshore) during the last  
399 week of October, 2010. Wave heights ( $H_{m0}$ ) less than 0.1 m not shown but corresponding peak  
400 periods ( $T_p$ ) are shown to reveal the low frequency nature. Bottom panel shows energy spectra  
401 highlighting bimodal nature of the wave field.

402

403 Figure 3 (a) Discrete and cumulative probability of observed sea and swell wave heights, (b)  
404 probability of observed peak wave periods and (c) probability of observed mean wave directions.

405

406 Figure 4 (a) Relative magnitude of shear stress produced by sea and swell compared to the  
407 relative magnitude of corresponding spectral energy. Size of the symbols scaled to spectral wave  
408 height of the whole un-partitioned spectrum. The values of  $kh$  are based on sea. (b) Frequency of  
409 occurrence of bed shear stress.

410

411 Figure 5 A scatter plot of ratio of bay swell height ( $H$ ) to offshore swell height ( $H_o$ ) against  
412 offshore swell height.

413

414 Fig. 6 Wave power and estimated erosion rate for waves coming *from* southeast quadrant  
415 (meteorological directions).

416

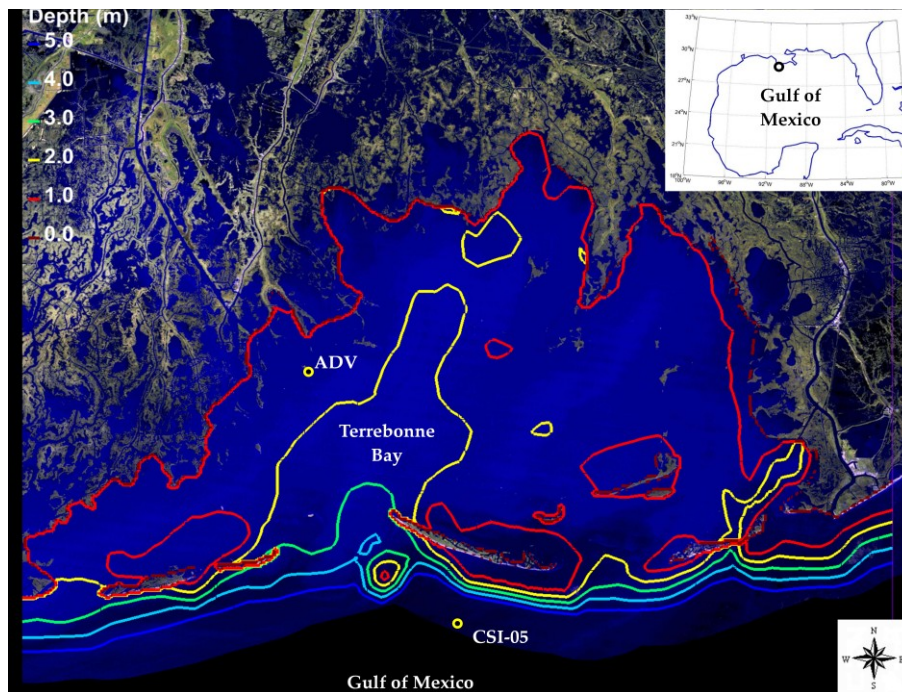


Fig. 1 Study area, bathymetry and locations of monitoring gages.

417

418

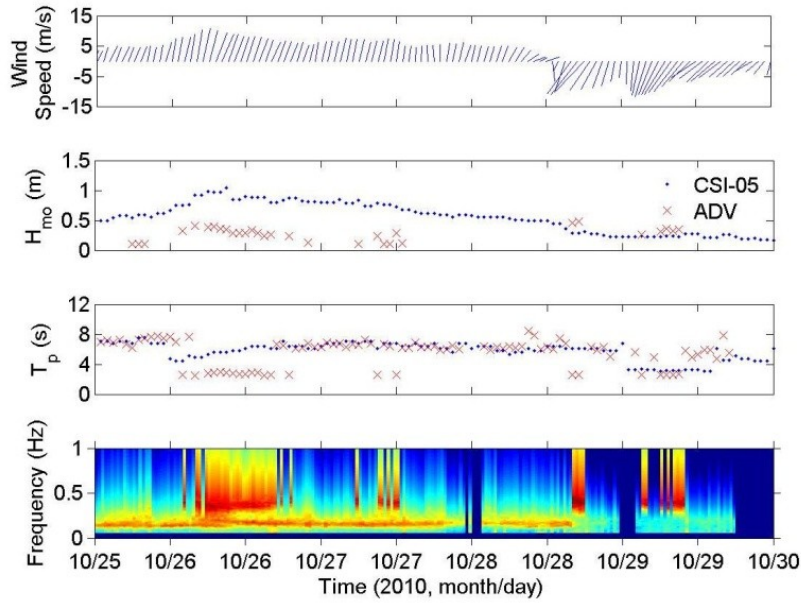


Fig. 2 Measured wave heights and periods at ADV (bay) and CSI-05 (offshore) during the last week of October, 2010. Wave heights ( $H_{mo}$ ) less than 0.1 m not shown but corresponding peak periods ( $T_p$ ) are shown to reveal the low frequency nature. Bottom panel shows energy spectra highlighting bimodal nature of the wave field.

419

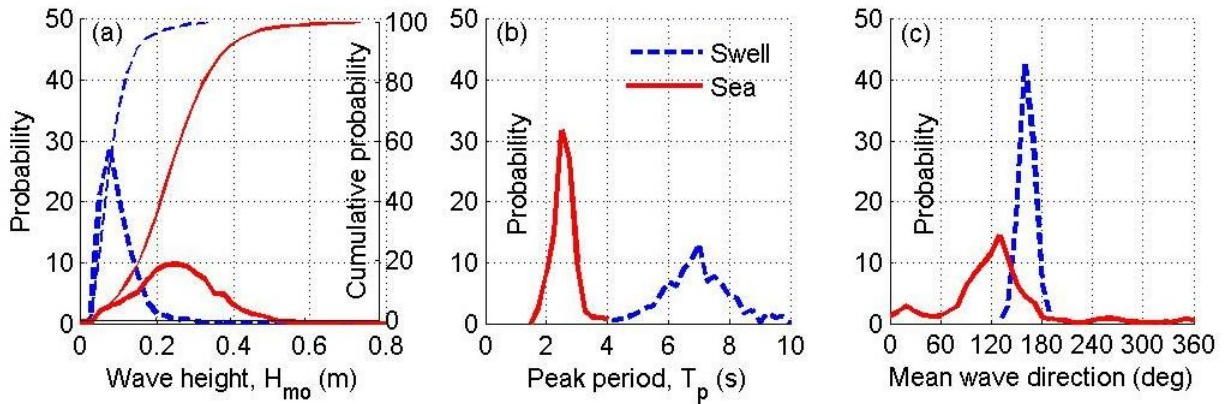


Fig. 3 (a) Discrete and cumulative probability of observed sea and swell wave heights, (b) probability of observed peak wave periods and (c) probability of observed mean wave directions.

420

421

422

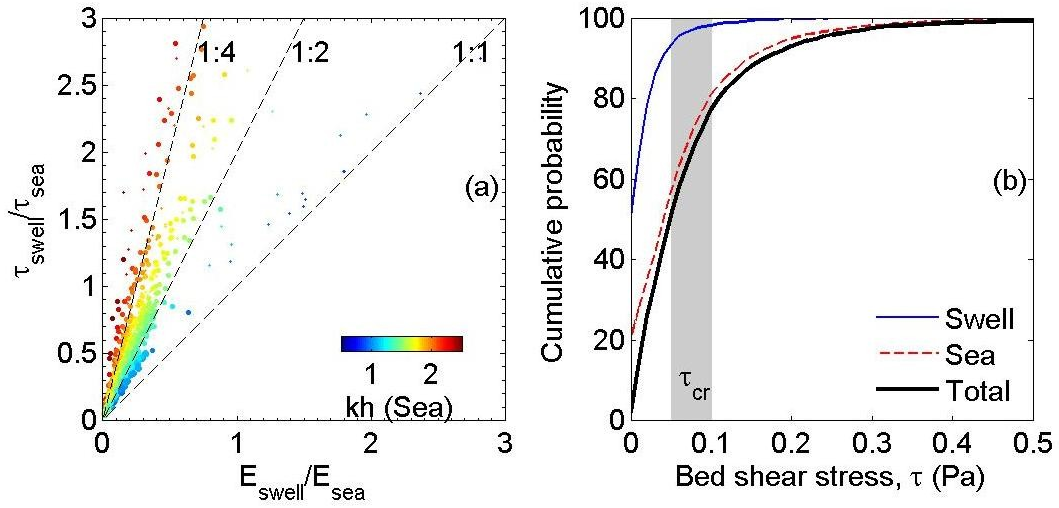


Fig. 4 (a) Relative magnitude of shear stress produced by sea and swell compared to the relative magnitude of corresponding spectral energy. Size of the symbols scaled to spectral wave height of the whole un-partitioned spectrum. The values of  $kh$  are based on sea. (b) Frequency of occurrence of bed shear stress.

423

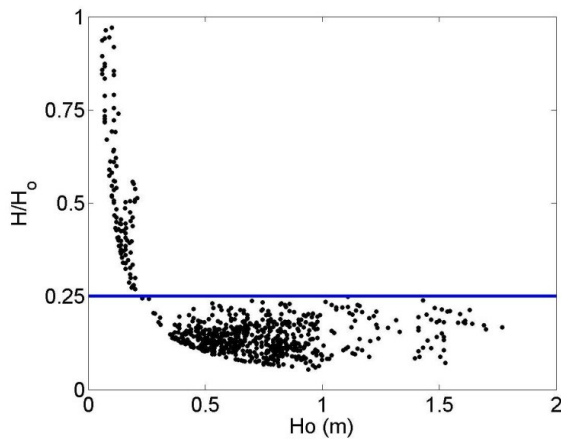


Fig.5 A scatter plot of ratio of bay swell height ( $H$ ) to offshore swell height ( $H_o$ ) against offshore swell height.

424

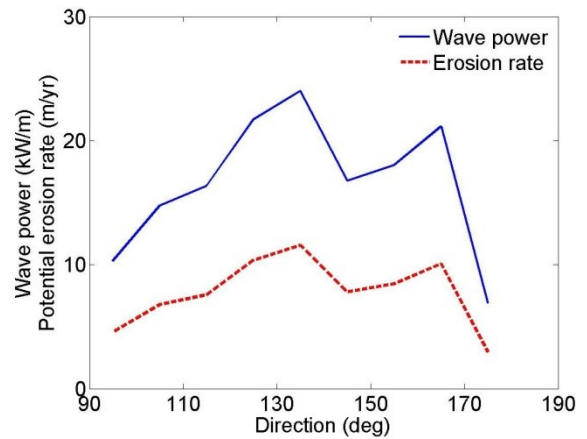


Fig. 6 Wave power and estimated erosion rate for waves coming from southeast quadrant (meteorological directions).